Tectonophysics 608 (2013) 376–388

Contents lists available at ScienceDirect

Tectonophysics

journal homepage: www.elsevier.com/locate/tecto

The role of lithospheric processes on the development of linear volcanic ridges in the Azores

M.C. Neves [a,*], J.M. Miranda [b], J.F. Luis [a]

[a] University of Algarve, IDL, Campus de Gambelas, 8005 139 Faro, Portugal
[b] Instituto Português do Mar e da Atmosfera, IDL, Rua C do Aeroporto de Lisboa, 1749 077 Lisboa, Portugal

ARTICLE INFO

Article history:
Received 26 April 2013
Received in revised form 9 September 2013
Accepted 12 September 2013
Available online 19 September 2013

Keywords:
Azores
Numerical modeling
Damage
Fracture
Linear Volcanic Ridge

ABSTRACT

Linear volcanic ridges (LVRs) are widespread along the Azores plateau and are often used as a tectonic marker of the surface stress field. Nevertheless, the mechanisms that drive the emplacement and development of these structures are not well established and they have been attributed to the plateau diffuse deformation, off-rift extension or the result of the interaction between a hotspot and the brittle lithosphere. This study hypothesizes that linear volcanic ridges are the result of magma emplacement into pre-existing damaged lithosphere, using a 3D finite-element representation of the brittle lithosphere and underlying ductile mantle, and assuming that the deformation is driven by plate boundary forces applied at the edges, as describe by global plate kinematic models. The brittle layer is described by an elastoplastic rheology with progressive damage, where fractures are assumed to be analogous to localized shear bands. The ductile mantle underneath is modeled as a viscoelastic layer that exerts a shear drag at the base of the brittle layer. The modeling shows that lithospheric processes alone can justify the spatial distribution of linear volcanic ridges, and even the development of the Faial Ridge. The factors controlling the fracturing pattern are the plate geometry and velocity boundary conditions, the shearing introduced at the East Azores Fracture Zone/Gloria fault limit and the interaction between the viscous mantle and the spatially varying brittle plate thickness. Along the Terceira Rift the predicted fractures match the orientation of the LVRs in the second (~N135°–N140°) and third (N150° to N–S) sectors and provide an explanation for the arcuate shape of the rift itself. The brittle plate thickness variations are crucial for the development of the more recent LVRs, which are predicted to occur along the Faial Ridge. In the best fit model the top mantle viscosity is 1×10^{22} Pa s at 5–15 km depth, and the present-day fracture network takes ~3 Ma to develop.

1. Introduction

A variety of geochemical and geophysical observations in the Azores have been attributed to the existence of a mantle hotspot (Schilling, 1975) or melting anomaly (e.g. Beier et al., 2008) and to its interaction with the Mid-Atlantic Ridge (MAR) (e.g. Cannat et al., 1999; Gente et al., 2003; Goslin et al., 1999). Seismic tomography studies have provided evidence for a low-velocity anomaly in the mantle beneath the Azores (e.g. Silveira et al., 2010; Yang et al., 2006) and the role of mantle dynamics has been emphasized in studies that address the effect of triple junction geometry on the excess of magmatism, and thereby, on the creation of the Azores plateau (Georgen and Lin, 2002; Georgen and Sankar, 2010). A recent model of mantle convection (Adam et al., 2013), based on tomography, predicts dynamic topography fitting the anomalous elevation of the Azores plateau and suggests two distinct mantle upwellings consistent with geochemical signatures observed in lava samples. The stresses induced by mantle convection at the base of the lithosphere are claimed to account for the tectonic regime and seismicity observations, but reasonable stresses are only obtained when a spatially varying lithosphere, not resolved by tomography, is incorporated. As in other regions of the world with volcanic systems, the tectonic and volcanic processes seem to be shaped by the interaction of a mantle plume with the overriding plate. In this study we try to explain part of the plateau's internal structure as a result of the vulnerability of the lithosphere to magma penetration due to lithospheric stresses imposed by plate boundary forces. This is a contribution to the ongoing debate of whether driving forces of the convective mantle or plate tectonic forces, together with geometry and structural heritage, control the plateau's internal structure, although a combination of driving mechanisms is likely required to explain the full range of observations.

According to Luis and Miranda (2008) the onset of the Azores extensional regime was triggered by the attachment of Iberia to Eurasia, following a major EU–AF–AM kinematic change between chron c13 (~33 Ma) and chron c6 (~20 Ma) (Fig. 1). This extensional process created a band of newly formed lithosphere, presently located close to Terceira Rift (Luis and Miranda, 2008) or Princess Alice basin (Miranda et al., 2013) (Fig. 2). The rest of the plateau is in fact oceanic crust formed

* Corresponding author at: Universidade do Algarve, FCT, ED8, Campus de Gambelas, 8005 139 Faro, Portugal. Tel.: +351 289800900x7361; fax: +351 2898000069.
E-mail address: mcneves@ualg.pt (M.C. Neves).

0040-1951/$ – see front matter
http://dx.doi.org/10.1016/j.tecto.2013.09.016

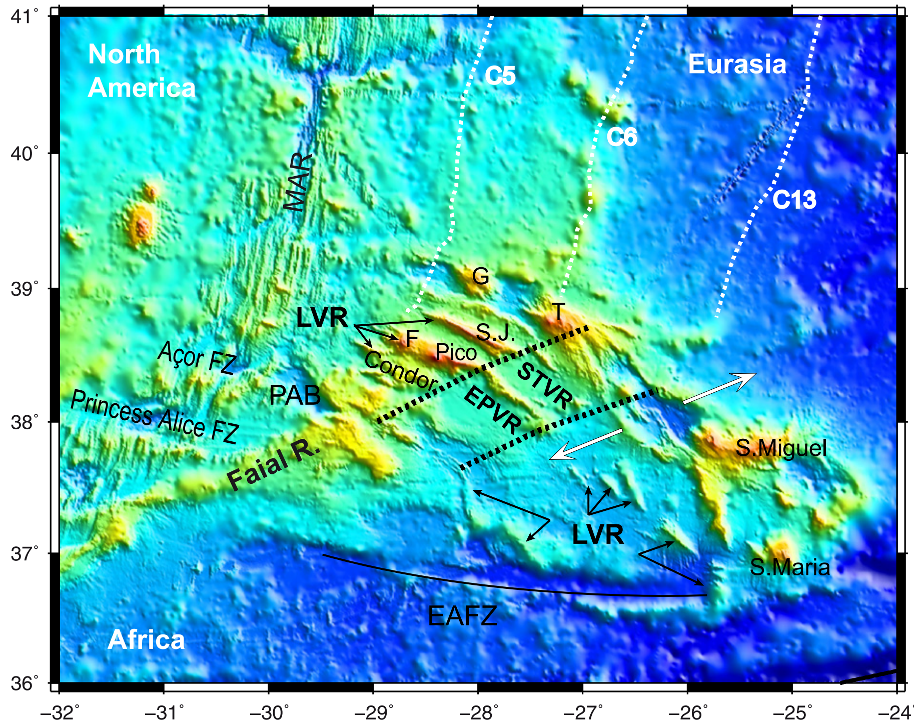

Fig. 1. The Azores plateau 250 m bathymetric grid. Linear Volcanic Ridge sectors are separated by black dotted lines. LVR: Linear Volcanic Ridge, EPVR: East Pico Volcanic Ridge, STVR: South Terceira Volcanic Ridge, Faial R.: Faial Ridge, F: Faial Island, G: Graciosa Island, S.J.: St. Jorge Island, T: Terceira Island, PAB: Princess Alice Basin, EAFZ: East Azores Fracture Zone, MAR: Mid-Atlantic Ridge. White dotted lines indicate isochrons c5 (~10.3 Ma), c6 (~19.6 Ma) and c13 (~33.3 Ma). White vectors between Terceira and S. Miguel islands indicate the relative motion between Eurasia and Africa at the time of chron c4 (~7.56 Ma), calculated from circuit closing using the finite poles of Luis and Miranda (2008). The relative motion at the time of chron c2a (~3.06 Ma), not plotted, has an almost identical direction.

at the MAR and later modified by magmatism and neo-tectonics. Since approximately chron c6 (~20 Ma) stretching is taking place at an average rate of ~3.8 mm/yr, progressively attaching Eurasian lithosphere to the African plate by a northward progression of the triple junction. In the meantime the relative velocity between Eurasia and Africa can be considered to have gone through 3 major stages: the first between 25 and 8 Ma, corresponding to the initial rifting of the plateau, the second between 8 and ~3 Ma, related to extension in the Princess Alice zone, and the third since ~3 Ma, corresponding to the Terceira axis rifting. The so-called Azores triple junction (TJ, Fig. 2) is at present a highly tectonized area of distributed deformation located close to 38° 55′N, 30° 00′W (Luis et al., 1994). The reanalysis of regional marine magnetic data for the north-Atlantic showed that south of 38° N African poles apply, north of 39.5° N Eurasian poles apply, and in between there is an almost continuous change between the two poles (Miranda et al., 2011). In this sense, there is no well defined plate boundary between Eurasia and Africa, but instead, the differential motion between the two plates, west of Western Graciosa basin is accommodated within a 100 km wide zone subject to right lateral transtension (Miranda et al., 2013).

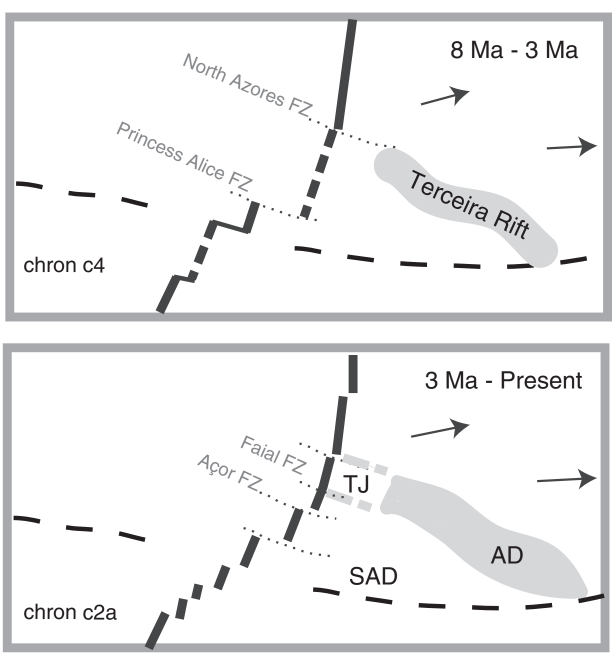

Fig. 2. Plate reconstitutions at chron c4 (~7.56 Ma) and c2a (~3.06 Ma) based on the magnetic re-evaluation of Luis and Miranda (2008). The two plate geometries simulate two distinct LVR initiation setups. The two setups are similar except for the MAR segmentation pattern and the velocity boundary conditions. SAD: South Azores Domain, AD: Azores Domain, TJ: Triple Junction area. Arrows indicate the relative motion between Eurasia and Africa.

The bulk of inter-plate deformation is presently focused on Terceira Rift (TR). However, a significant amount of intraplate deformation develops off-rift, corresponding to São Jorge and the Faial–Pico islands. The morphostructural analysis of Lourenço et al. (1998) interpreted this area of the plateau as a transtensional domain where rifting processes, in pure tension, coexist with the development of NNW–SSE left lateral shear faults and WSW–ENE relay zones. Nearly 90% of all mapped fault scarps, lineations and elongated seamounts, widespread along the Azores plateau, have azimuths between 100° and 160°. Within this range the two most frequent strikes are 110°–120°, at west, and 140°–150°, at east, in agreement with the arcuate form of the Terceira axis itself. These two directions establish the framework for the distribution of volcanism expressed either as point source volcanism or Linear Volcanic Ridges (LVRs). The LVR or elongated seamounts develop along fissure systems and are the most pervasive form of volcanism. Islands like S. Jorge, Pico and Faial are extreme cases of LVR development. The point source volcanism consists of circular edifices believed to originate at the intersection of tectonic structures with both directions (Guest et al., 1999).

The LVRs have been classified into three different categories or sectors (Lourenço, 2007; Lourenço et al., 1998). The first encompasses the S. Jorge, Faial and Pico islands and two co-planar linear volcanic ridges designated as the "Condor" ridges, all showing a nearly uniform axial orientation of N120° and consistently positive magnetic anomalies along their strike (Miranda et al., 2013). The second LVR category comprises the East Pico Volcanic Ridge (EPVR), the South Terceira Volcanic Ridge (STVR) and several other volcanic ridges further south, all showing axial orientations of ~N135°–N140° and complex magnetic signatures, occasionally masked by MAR generated magnetic anomalies. Finally, the third is found south of the S. Miguel Island, and shows predominantly N150° and N–S orientations. This sector includes the sharply bended LVRs that root in the East Azores Fracture Zone (EAFZ).

Currently active structures have been identified and characterized based on the joint interpretation of acoustic facies from sonar TOBI images and high resolution magnetic anomaly maps (Lourenço et al., 1998). The overall magnetic and morphotectonic analysis indicated that LVRs in the first sector are more recent and active than LVRs in the second and third sector: LVRs in sector 1 show more active volcanic features, with consistently positive magnetic anomalies along their strike, whereas LVRs in sectors 2 and 3 present a more complex magnetic anomaly pattern and less robust active volcanism; in sector 1 there is evidence of ridge propagation westwards, such as graben development west of S. Jorge tip and submarine prolongation of the fissural system in Faial, whereas such propagation evidence is absent in sectors 2 and 3; finally, the main area of earthquake activity is currently located west of sector 1.

Vogt and Jung (2004) suggested that LVRs are traces of failed rifts, the TR being the most recent of these rifting events. Their premise is that rifting is forced to jump in response to the SW absolute motion of the EU–AF plate boundary over the Azores hotspot. These authors suggest that the arcuate shape of the TR may result from the relocation of active spreading in response to the emplacement of massive volcanic loads or tectonic piles. Such a mechanism seems valid at a broad scale, to explain the northward migration of the triple junction. However, the age progression it implies for the LVRs, progressively younger towards NE, does not fit observations because it does not explain the actual concentration of tectonic and volcanic activity in the first LVR sector. Thus, we need an alternative mechanism explaining why the LVRs are more active towards northwest.

The pattern of linear volcanic ridges was used by Lourenço et al. (1998) as a marker of the tectonic stress field. They qualitatively interpreted it as a result of the prevalence of co-axial oblique extension, focalized within the Terceira axis, and a stress field with minimum compressive axis sub-parallel to the opening directions predicted by geological and geodetic kinematic models (Fig. 1).

Despite the existing LVR interpretations (Lourenço et al., 1998; Vogt and Jung, 2004) the LVR development has never been addressed quantitatively. The aim of this study is to provide a consistent explanation for the LVR growth and for the birth of the TR using numerical modeling techniques. The transport of magma through the brittle part of the lithosphere is considered to occur via fractures. We try to determine the most likely paths of fracture development using a 3D representation of the brittle lithosphere and underlying ductile mantle, driven by plate boundary forces applied at their edges. The brittle layer is governed by an elastoplastic rheology with progressive damage where fractures are assumed to be analogous to localized shear bands. Rheologies based on continuum damage mechanics (e.g. Lemaitre, 1992) enable simulations of long-term lithospheric shear localization leading to fracture nucleation and evolution (Lyakhovsky et al., 1997; Rudnicki and Rice, 1975) and have been able to predict the formation of shear bands on a wide range of scales (Bercovici et al., 2001; Finzi et al., 2012; Hieronymus, 2004). Here we use an elastoplastic damage rheology to predict the patterns of fracturing, and thus of LVRs, at the scale of the Azores triple junction.

2. Modeling description

Modeling is done with a commercial finite element package (ABAQUS/Explicit) that uses the explicit forward Euler algorithm and a large-displacement formulation. ABAQUS is able to solve problems involving complex contact interactions and material degradation after failure, thus suitable to analyze the progressive evolution of damage. The details of the numerical modeling formulation are given in Appendix A. Here we focus on the design and description of the models.

2.1. Conceptual 2D models

The 2D models demonstrate the modeling principles and put into evidence our two main premises: a) shearing in the Azores can drive a curved crack resembling the TR and b) variations in brittle thickness enhance damage and help to localize fractures and LVRs.

The first model corresponds to a 2D horizontal plate loaded in extension and shear (Fig. 3). Extension is driven by velocity boundary conditions applied at the top and right-hand sides. Shear is created by the boundary velocity discontinuity (no slip/slip) at x = 500 km, y = 0, which simulates the East Azores Fracture Zone/Gloria fault discontinuity. A plane stress approximation (no gravity) and the Von-Mises plasticity criterion (no depth or pressure dependency) are assumed. The plate's material rheology, elastoplastic with damage, is otherwise described in Appendix A. The predicted crack corresponds to a damage zone that starts at the discontinuity. The damage trajectory is at each point perpendicular to the minimum compressive stress, and therefore it curves

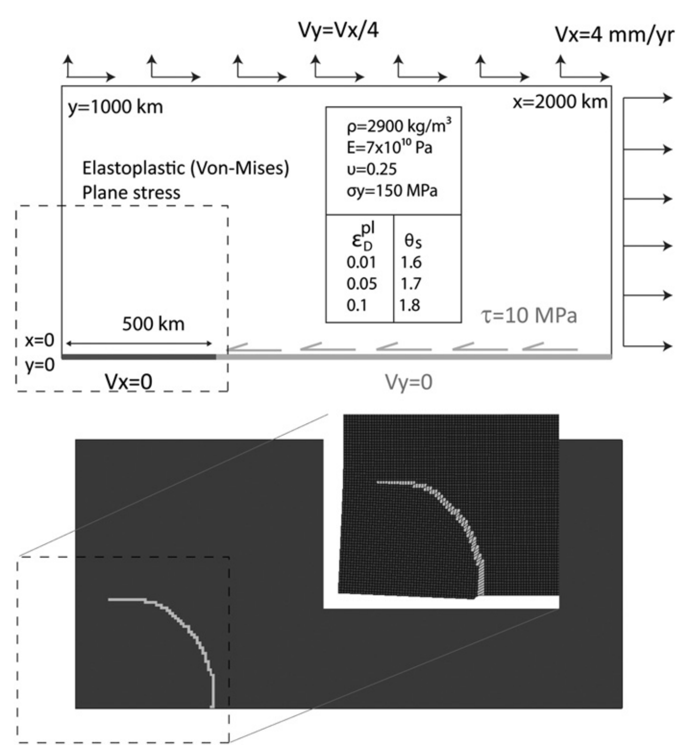

Fig. 3. Setup and results of a 2D finite element plate model loaded in extension. The rheology is elastoplastic with damage with parameters (defined in Table A.1 of Appendix A) shown in the inset (σy is the Von Mises yield stress). Predicted fracturing is depicted as a plot of the damage variable (light gray elements where D = 1) with the close up showing the fracture path in a deformed mesh frame. The curved crack develops due the boundary condition discontinuity (slip/no slip) at y = 0, which simulates the EAFZ/Gloria fault discontinuity.

according to the stress pattern. Although no friction along the slipping section at y = 0 is needed to induce the crack, in this example we have imposed a shear stress of 10 MPa. In fact the curvature of the crack increases with the magnitude of the applied shear stress.

The second model corresponds to a 2D plane strain vertical section of the crust, comprising a brittle layer, with a variable thickness region, on top of a ductile layer (Fig. 4). The rheologies, elastoplastic (Drucker–Prager) with damage and viscoelastic, as well as the loads and the boundary conditions, are similar to those of the benchmark problem described in Appendix A. The modeling results show that the brittle thickness variation provides the heterogeneity necessary to drive shear band localization. The predicted damage trajectory starts at the edge of the dipping boundary and forms a shear zone that obeys Coulomb law. The larger the brittle thickening gradient the easier it becomes to develop the damage zone. Tests have shown that a similar pattern of fracture development is predicted for a motionless (Vx = 0), or resisting, viscoelastic layer.

2.2. The Azores 3D model

The 3D models integrate both features of the previous 2D models: a velocity discontinuity at the EAFZ/Gloria fault intersection and brittle thickness variations. They represent two initially undamaged configurations of the Azores tectonic setting (Fig. 2). The first model is based on the plate reconstructions at the time of chron c4 (~7.56 Ma), when presumably fracturing leading to LVR formation began, contemporaneously or just after extension in the Princess Alice region. The second model incorporates the present-day MAR segmentation and represents the tectonic setting in the last 3 Ma, since approximately chron c2a (~3.06 Ma). It simulates the hypothesis of the very recent (<3 Ma) fracturing and LVR construction, consistent with age determinations showing that with the exception of Santa Maria island, volcanism in the Azores is less than ~2 Ma old (Hildenbrand et al., 2012).

Apart from the MAR segmentation the geometry of the two 3D models is identical and contains two parts, Eurasia and Africa, which are connected along the EAFZ and interact along the Gloria fault (Fig. 5). The northern and eastern boundaries of Eurasia are at more than 500 km from the Azores archipelago to prevent boundary effects. The finite element mesh is unstructured and composed of quadratic elements with a minimum length of 5 km. Since the LVRs we want to simulate as damage zones are about 10–20 km wide, this means that the element size is less, or approximately the same, than the target damage bandwidth. The sensitivity of the results to the finite element mesh (type and resolution) is analyzed in Section 4.1.

The models are 100 km thick in the vertical, and are composed of two layers. The upper layer behaves like a quasi-brittle material subjected to plastic deformation, which can localize and form shear zones and fractures. The ductile mantle below is a highly viscous fluid governed by a linear viscoelastic law. The base of the elastoplastic plate is assumed to roughly coincide with the brittle–ductile transition defined by the 400 °C isotherm. The elastic thickness (T_e) contours shown in Fig. 5 represent the 400 °C isotherm depth estimated from the relation: $1.5 + 2.7\sqrt{t}$, where t is age in Ma (Parsons and Sclater, 1977) corrected to take into account the residual bathymetry. In Section 4.3 we address the sensitivity of the model results to variations in the elastic plate thickness. The average elastic plate thickness in the region of the Azores archipelago is ~7.5 km which is consistent with estimates from gravity studies (e.g. Luis and Neves, 2006).

The motion of Eurasia relative to fixed Africa is prescribed as velocity boundary conditions applied to the northern and eastern plate boundaries. The velocities are calculated according to the Eurasia/Africa Euler poles at the time of chron c4 (~7.56 Ma) and chron c2a (~3.06 Ma). These have been determined from circuit closing using the finite poles for the Eurasia/North America, computed by Luis and Miranda (2008), and Africa/North America (unpublished, ongoing work). No boundary conditions are applied along the Eurasia western boundary (MAR) based on the assumption that mid-ocean ridges are weak and cannot sustain significant deviatoric stress. Moreover, we verified that applying a small extensional force at this boundary does not significantly change the results. The whole model is subjected to gravity. The Gloria fault is modeled as a contact surface with tangential frictional behavior. The effect of changing the value of the coefficient of friction is described in Section 4.2. The top of the model is a free surface. The lateral sides of Africa and the base of the model have free slip boundary conditions.

The rheologic parameters of the damage elastoplastic layer, namely the strain localization thresholds, are subjected to great uncertainty and have little experimental support. Plastic strain thresholds varying between 0 and 1.0 are reported in finite element simulations of strain localization, based on friction angle or cohesion softening (e.g. Ellis et al., 2004; Kaus, 2010). We conducted a search parameter analysis around the values displayed in Table 1 to find the best fit models. The corresponding sensitivity analysis is described in Section 4.3. The rheology of the layer underneath the brittle plate is viscoelastic with a viscosity that decreases linearly with depth at a rate of ~0.1 Pa s/km. The sensitivity of the results to the mantle viscosity values is also analyzed in Section 4.3.

3. Analysis of modeling results

In the upper brittle layer the extent of damage is illustrated by the scalar damage variable D, which represents the material stiffness degradation associated with failure (see Appendix A for details). The

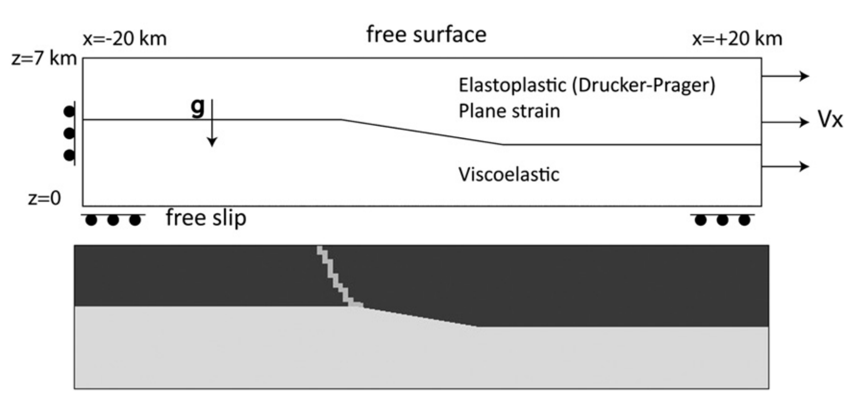

Fig. 4. Setup (see Table A.1 of Appendix A for material parameters) and results of a 2D vertical model of the crust and mantle. The interaction between the viscous and the elastoplastic layer is perturbed by layer thickness variations. A dipping section or a step in the layer's interface produces a heterogeneity that drives localization and damage in the upper layer. The predicted fracturing is depicted as a plot of the damage variable (light gray elements where D = 1) as in Fig. 3.

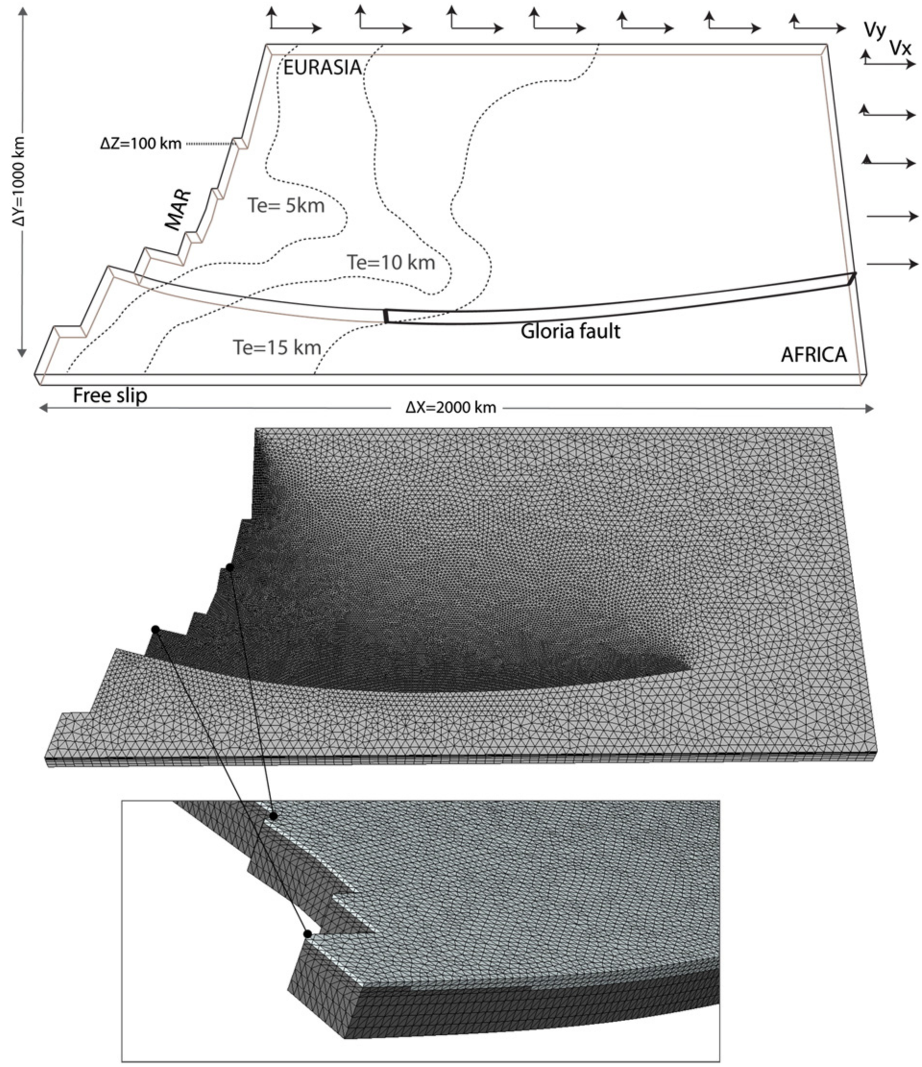

Fig. 5. Three-dimensional finite element model and mesh. The model contains an upper brittle layer and a lower ductile layer discretized into an irregular mesh with a minimum element length of 5 km. The close-up shows the grid in the SW corner of Eurasia. The base of the brittle layer, defined by the elastic plate thickness (Te), varies between 5 and 15 km. Eurasia and Africa interact along the Gloria fault, defined as a contact surface. Velocity boundary conditions $\left(\vec{V}\right)$ consistent with a fixed African plate, are indicated by black arrows. Free slip boundary conditions apply at the lateral sides of Africa and at the bottom of the model.

predicted localized shear bands (or damage zones) are places of maximum material degradation which are to be compared with the observed LVRs.

Table 1
Parameters used in the 3D models.

	Parameter	Value
Gloria fault	Friction coefficient	0.6
Viscoelastic layer	Density (ρ)	3300 kg m^{-3}
	Viscosity (η) [top, bottom]	[1E22, ~1E21] Pa s
	Young's modulus (E)	1E11 Pa
	Poisson's ratio (ν)	0.45
Elastoplastic layer	Density (ρ)	2900 kg m^{-3}
	Young's modulus (E)	1E11 Pa
	Poisson's ratio (ν)	0.25
	Coulomb friction angle (φ)	35°
	Coulomb cohesion (c_0)	50 MPa
	Dilation angle (Ψ)	35°
	Damage initiation criterion ε_D^{pl},θ_s (in tabular form)	(0.01,1.8),(0.05,2.2) for $\dot{\varepsilon}\epsilon$ [0, 1], (0.1,2.6)
	Displacement at failure (u_f^{pl})	0.001
Solution control	Loading rate acceleration factor	1×10^7 s
	Explicit time increment (element size)	0.016 s (10 km × 5 km)

3.1. Pattern of LVRs

The location of the maximum D values (D = 1, black lines) is superimposed on the bathymetry (Fig. 6) to highlight the comparison between the predicted shear zones and the Azores volcanic–tectonic fabric. The model corresponding to the chron c4 tectonic setting has a constant brittle layer thickness (Te = 10 km) in order to address the effect of the boundary conditions on a pristine plate. It shows two distinct damage zones, with approximately N120° and N150° orientations. The N120° structure is related with the MAR offset whereas the N150° structure is related to the Gloria fault limit. These numerical predictions exhibit good qualitative agreement with the morphological and magnetic information supporting the existence of only two major rift features (the princess Alice and the Terceira Rifts) in the Azores plateau (Miranda et al., 2013).

The model corresponding to the chron c2a (actual) tectonic setting has variable brittle thickness (see Te distribution in Fig. 5). The predicted fractures match reasonably well the observed LVRs, with predominant strikes varying between N120° and N150°. Damage zones grow along the V-shaped Faial ridge, suggesting a link between the formation of the Faial Ridge, the brittle layer thickening and the MAR segmentation. Also, in the actual setting the Princess Alice rift is less developed and

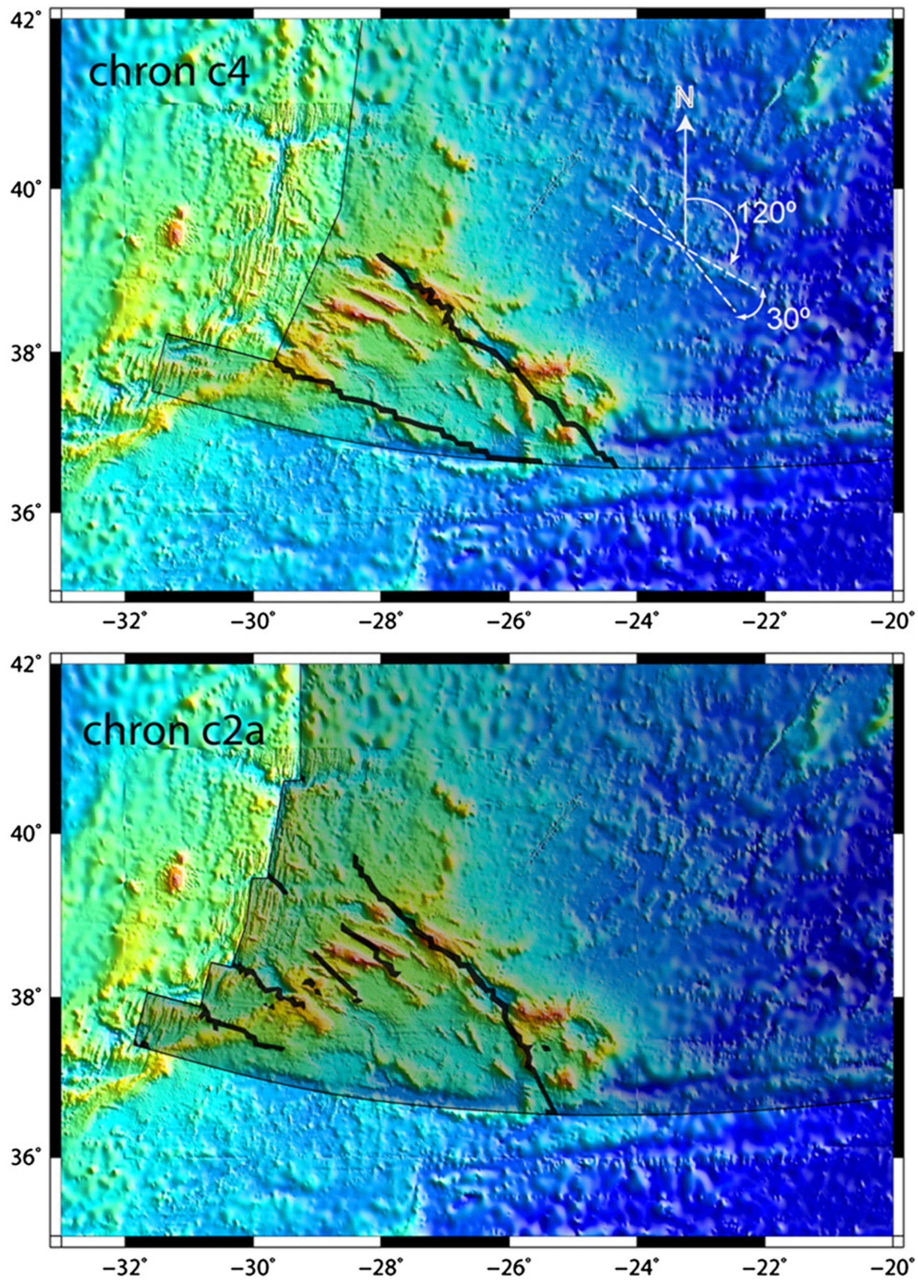

Fig. 6. Model results (parameters shown in Table 1) for the chron c4 and chron c2a tectonic settings. The predicted damage (black elements where D = 1) is superimposed on the Azores bathymetry to highlight comparison between fracturing and LVRs. The chron c4 model has constant brittle plate thickness (Te = 10 km) and the chron c2a model has variable Te (as depicted in Fig. 5). Plate geometry, brittle thickness variations and boundary conditions control the individual trends of the predicted damage zones. These fit most of the observed morpho-tectonic trends with dominant N120° and N150° directions. The Faial Ridge growth is favored in the present MAR segmentation pattern and there is a gap between the predicted LVRs and the MAR to the north of the Açor Fracture Zone.

the TR stands out as the major active structure. This numerical result reproduces the present day location of the rifting processes in the Azores, as demonstrated by magnetic, seismotectonic and space geodetic data. The model also predicts the arcuate shape of the Terceira axis, and represents particularly well the orientation of the LVRs in the second (~N135°–N140°) and third (N150° to N–S) sectors. The discrepancy relative to the N120° orientation of the first LVR sector can be attributed to the neglecting of the local stress field near the MAR. Earthquakes and active normal faulting near mid-ocean ridges indicate an extensional regime arising from a stress deficiency at the ridge axis relative to the lithostatic state of stress (e.g. Lachenbruch, 1973; Lin and Parmentier, 1990). This extensional regime, characterized by ridge-parallel and ridge-perpendicular stress orientations (e.g. Neves et al., 2004), was not simulated here and could contribute to a local rotation of the predicted LVRs near the MAR.

3.2. LVR evolution

There are two competing processes controlling the timing and sequence of damage, which are evidenced in the 2D conceptual models: (1) the development of the Terceira axis crack and (2) the fractures induced by the brittle thickness variations. Rather than being isolated features these fractures tend to form arrays but their onset time is dependent on the rheologic parameters (mainly the viscosity of the upper mantle and the strain localization threshold of the upper brittle layer). For example, for low viscosity values or low shear strain localization thresholds, the fractures aligned along the Faial ridge may develop at the same time, or even before, than the TR crack.

The evolution of LVRs may be considered analogous to the progression of rifting in extensional plate boundaries. Extension is initially accommodated by stretching and faulting and subsequently partially accommodated by dyke intrusions that help to localize strain during repeated rifting episodes (e.g. Beutel et al., 2010; Keir et al., 2006). Although the partitioning of strain between faults and magmatic intrusions is not always clear, currently active rifts are unquestionably places where magmatic and tectonic activity concentrates.

Taking into consideration the actual concentration of the volcanic and tectonic activity in the first LVR sector, we favor a model in which the TR predates the Faial ridge alignments, which include the Pico, Faial and S. Jorge islands. This places constraints of ~1×10^{22} Pa s for the upper mantle viscosity at 15 km depth and of ~0.01 for the minimum strain localization threshold. These are the values used in the chron c2a model (Fig. 6), which is the one that best fits the morphological observations. The corresponding evolution of the damage network (Fig. 7) shows that the TR is the first damage zone to form (time T1), emanating from the EAFZ/Gloria fault discontinuity. At a later stage (time T2) the damage develops almost simultaneously along concurrent paths, forming en-echelon fracture arrays. They align along the Faial ridge with trends varying between N120° and N150°. These damage zones increase in length as propagating cracks that

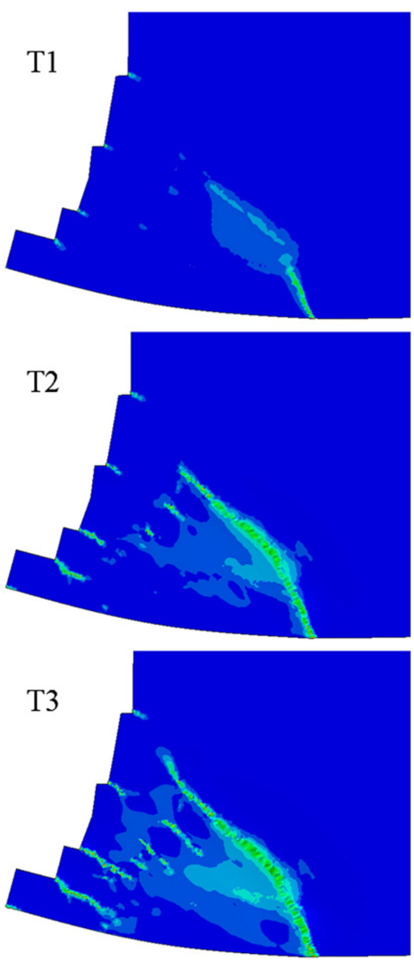

Fig. 7. Evolution of the fracture pattern for the chron c2a setup (final stage shown also in Fig. 6). The sequence shows plots of the shear initiation criterion (as Fig. A.2—Appendix A) and the green color indicates full degradation or damage. As the present day tectonic activity concentrates in the first LVR sector (comprising S. Jorge, Faial and Pico islands) we favor a model in which the initiation of the Terceira Rift (at time T1) is followed by the creation (at time T2) and latter growth (at time T3) of the Faial Ridge structures. For an LVR width of ~10 km (damage bandwidth) and top mantle viscosity of ~1×10^{22} Pa s the timing is T1 = ~1 Ma, T2 = ~2 Ma and T3 = ~3 Ma.

grow due to stress concentrations at their tips. They lengthen away from central portions advancing towards the MAR and the EAFZ. Nonetheless, the propagation of damage towards the MAR is inhibited beyond the Faial ridge, especially to the north of the Açor Fracture Zone (time T3).

The timing for the onset of damage also depends on the numerical time step, which is a function of the mesh resolution (Appendix A). Nonetheless, for damage bandwidths between 5 and 20 km, representative of the observed LVRs, the onset times are very similar. The results described here are obtained for a damage bandwidth (horizontal resolution) of 10 km. In this case T1 = ~1 Ma, T2 = ~2 Ma and T3 = ~3 Ma, and thus the essential of the damage network develops in the first 3 Ma.

4. Sensitivity analysis

During the course of the modeling we examined the effect of several parameter values in the solution. Here we focus on the most critical ones.

4.1. Sensitivity to the FEM mesh

The mesh sensitivity is a well identified problem in numerical simulations of shear localization (e.g. de Borst, 2002; Buiter et al, 2006; Crook et al., 2006). Consider a model without Gloria fault, with an upper mantle viscosity of 1×10^{22} Pa s and minimum strain localization threshold of 0.01. The predicted damage pattern using three different FEM grids is shown for: (Fig. 8a) hexahedral elements with second order accuracy (C3D8R) and average horizontal resolution of 10 km; (Fig. 8b) quadratic tetrahedral elements (C3D10M) and average horizontal resolution of 10 km; and (Fig. 8c) quadratic tetrahedral elements with average horizontal resolution of 5 km (aspect ratio 1:1). Finer resolutions would be computationally unreasonable. As can be observed the solutions display a common pattern in spite of being sensitive to the FEM discretisation. In fact, some variability in the predicted damage patterns is generally accepted as reflecting the inherent variability in the fault forming process. In any of these models the damage network takes ~2 Ma to develop.

4.2. Sensitivity to loading conditions

The models described in Section 4.1 demonstrate that LVRs may form even in the absence of the EAFZ/Gloria fault discontinuity. The model shown in Fig. 8d has a constant brittle thickness of 15 km and the same material parameters as before, but includes the Gloria fault with a coefficient of friction of 0.6. The obtained fracturing pattern is incipient, occurring in the vicinity of the Princess Alice and Açor Fracture zones, and at the eastern end of the Terceira axis. It demonstrates that the structures observed near 25° 40′W, and the arcuate shape of the TR in the east, can be attributed to the presence of the Gloria fault. We also run a suit of models with different friction coefficient along the Gloria fault (varying between 0.3 and 0.8) but they produced similar damage patterns and timings of onset of the TR (~1 Ma). The time needed for the fractures to grow is however much longer than in Section 4.1 (~9 Ma).

The velocity of Eurasia relative to Africa during the two modeled time periods (chron c4 and chron c2a) is similar enough to produce no appreciable difference in the modeling results. Nonetheless, tests have shown that the Y component of the velocity, causing stretching across Azores Domain, is the one that most influences the damage pattern.

4.3. Sensitivity to rheological parameters

Localized shear bands also form in models with uniform elastic thickness, as Fig. 8d shows. Heterogeneities are essential for damage

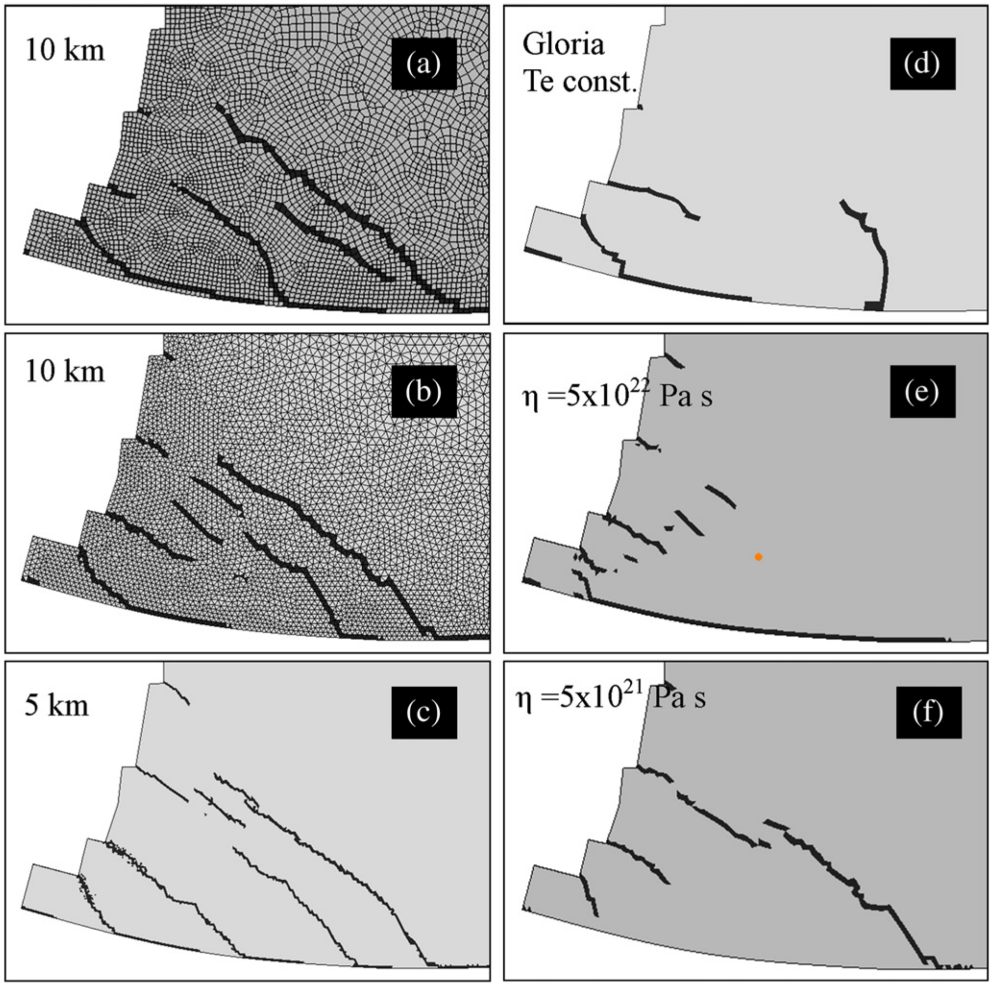

Fig. 8. Sensitivity analysis of the numerical model. Diagrams (a)–(c) shown after 3 Ma, (d) after 9 Ma, (e) after 6 Ma and (f) after 1.5 Ma (note that these are total times, not timing of onset of the structures). With exception of panel (d), which includes the Gloria fault in a constant thickness plate (Te = 15 km), all other models have variable brittle thickness but no Gloria fault. Panels (a)–(c) demonstrate the effect of the finite element mesh, (d) the effect of the Gloria fault and (e)–(f) the effect of the top mantle viscosity.

nucleation, but once strain localization zones are nucleated, their propagation path and final trend are determined by the stress field rather than by the heterogeneity itself. As a consequence the final pattern of LVRs is not very sensitive to changes in the actual distribution of elastic plate thickness.

In models with variable brittle thickness (Te) the pattern and timing of fracturing are mainly determined by the upper mantle viscosity. Models in Fig. 8e and f are identical to Fig. 8b (do not include Gloria fault), except that they have different mantle viscosity profiles. We observe that larger viscosity values favor the development of LVRs along the Faial ridge (Fig. 8e) whereas smaller viscosity values favor the development of the Princess Alice and Terceira Rifts (Fig. 8f). The time needed for the development of the Faial ridge structures is ~6 Ma for an upper mantle viscosity of 5×10^{22} Pa s, whereas the time needed for the development of the Terceira and Princess Alice damage is ~1.5 Ma for an upper mantle viscosity of 5×10^{21} Pa s. Outside this range of top mantle viscosity values, the modeling results do not reproduce the LVRs. Thus, larger viscosities do not generate damage at the time scale of the observed structures (<10 Ma) and smaller viscosities generate too much damage leading to sudden widespread fracturing.

The damage initiation criterion (Appendix A) is mostly controlled by the minimum strain localization threshold, since the shear stress ratio θ_s is mainly determined by the loading and boundary conditions. In the modeled tectonic setting the minimum strain localization thresholds producing acceptable results lie in the range between 0.01 and 0.1. Tests have also shown that the Drucker–Prager cohesion and friction angle are not critical parameters.

5. Discussion

5.1. What controls the plateau internal structure?

The observations regarding the internal structure of the Azores plateau (LVRs, faults, earthquakes), used as stress field indicators, occur in the brittle or rigid part of the lithosphere. According to these observations the Azores is in a broad transtensional regime characterized by curvilinear trajectories of the maximum and minimum compressive stresses (see Fig. 8 of Lourenço et al., 1998), where the maximum compressive stress trace rotates from ~N120° near the MAR to nearly N–S near the EAFZ. Our predicted fracture network agrees with these observations as damage zones align with the maximum compressive stress. In this sense our results confirm previous tectonic interpretations in which magma transport in the Azores region is mainly controlled by lithospheric architecture and tectonic stress (Lourenço et al., 1998).

Nonetheless, recent models of mantle convection in the Azores (Adam et al., 2013), driven by deep seated (>100 km depth) density anomalies, are also able to predict the overall stress pattern observed at surface. So we are back to the question of whether plate tectonic forces or mantle convection controls the tectonic stress. In Adam et al.'s (2013) study the mantle convection pattern fits well the dynamic topography and rifting direction west of Terceira Island, but only produces a fit to the observed stress pattern when the model incorporates a rigid lithosphere (defined by the 1200 °C isotherm), with variable thickness based on the observed isochron distribution of Luis and Miranda (2008). In our model the brittle/viscous interaction (at the depth of the 400 °C isotherm) occurs in a mantle with uniform velocity distribution, well justifying off-rift deformation in the Azores plateau and the development of the eastern segment of TR, but the fit to observations east of Terceira island is not so good. Apparently both processes cooperate: mantle dynamics was relevant for the development of the plateau and is still constraining rifting, particularly in the western segments of TR, while global plate tectonic forces determined the timing and amount of rifting, the segmentation of TR, and created a fracturation pattern, particularly off-rift, that drives the emplacement of linear volcanic ridges. The development of the large volcanic systems that form the islands is a consequence of mantle processes, but their emplacement and evolution is strongly constrained by lithospheric rifting.

5.2. Implication for the Terceira Rift development

Along the TR the fissural system is continuous enough to form a succession of volcanic massifs and inter-island basins which may simply be regarded as unfilled rift valley segments (Saemundsson, 1986; Vogt and Jung, 2004). To explain the geometric relations observed between volcanic edifices and tectonic structures in Terceira Island, regardless of their spatial scale, it has been proposed that en-echelon extension fractures, deep enough to reach melted rocks, form along deep-seated vertical fault zones reactivated by transtensional strike-slip motion (Navarro et al., 2009). Our localized shear bands modeled as damage zones can be considered as these deep-seated fault zones, or the precursors of continuous rifts along which focused volcanic eruptions occur. Age determinations in the Azores indicate that all islands, with the exception of St. Maria Island, are younger than ~2 Ma and have no coherent age progressions (Hildenbrand et al., 2012; Johnson et al., 1998; Silva et al., 2012). In fact, all evidence points to a process of LVR and island construction dominated by episodic fissural eruptions (Stretch et al., 2006) whose size and frequency depend on melt availability and tectonic stress.

Our models indicate that LVRs, which are recent structures probably less than 2 Ma old, occur along fractures induced by brittle thickness variations and mantle drag. This fracturing is simultaneous and widespread (Fig. 8a–c) and supports the absence of coherent age progression data. At an earlier stage of the plateau evolution, the chron c4 (~7.56 Ma) model (Fig. 6) indicates that plate geometry and kinematics may alone have generated two initial rifting events, along the Princess Alice and Terceira Rifts. Volcanism along these initial rifts may be responsible for modifying the normal thermal subsidence and for creating the brittle thickness variations that are inferred at present. Although an anomalous amount of melt production over a relatively long period is required to explain the anomalous crustal thickness and overall abundant volcanism in the Azores, our results demonstrate that rifting of the upper brittle lithosphere, consistent with the Terceira axis trend, may have occurred without the need of enhanced magmatic pulses related to mantle plume activity.

It has been recognized that widely spaced volcanoes and non-linear age progressions may be due to the interaction of magma transport and lithospheric flexure (e.g. Ten Brink, 1991). According to Vogt and Jung (2004) a similar argument based on flexural stresses may account for the arcuate shape of the TR. Other ultra-slow spreading ridges, like the Mohns–Knipovich Ridge, Gakkel Ridge, Southwest Indian Ridge, and Aegir Ridge, also have a volcanic–avolcanic segmentation pattern forming an irregular and widely curved configuration (see Fig. 4 of Vogt and Jung, 2004). According to our results the TR arcuate shape, in particular to the east of S. Miguel Island, is analogous to the curvature of a crack born at the Gloria fault limit. In order to gain full insight into the development of the Terceira axis, and possibly other arcuate shaped ultra-slow-spreading ridges, further investigations ought to combine mantle plume and lithospheric fracture simulations.

6. Conclusions

It has been suggested in previous studies that the Azores LVRs are failed or abandoned rifts created by the SW motion of the Eurasian plate over the Azores hotspot. In this study we show that LVRs, and the fracturing pattern that constitutes the Azores plateau internal structure, can also be explained by plate tectonic mechanisms. We consider LVRs and the Azores volcanism in general as being of fissural type, and present a model of fracturing of the Eurasia plate driven by plate kinematics and boundary forces. The upper brittle lithosphere is treated as an elastoplastic layer with progressive damage, and localized shear bands, or damaged zones, are interpreted as faults. The modeling predicts a fracture network with dominant trends varying between N120° and N150°, consistent with the observed LVRs, especially along the Faial ridge and TR. The factors controlling the fracturing pattern (under the extension imposed by velocity boundary conditions) are the shearing introduced at the EAFZ/Gloria fault limit and the interaction between the mantle drag and a spatially varying brittle plate thickness.

We conclude that kinematics and plate geometry can alone account for breaking the upper brittle lithosphere in the Azores in the last 10 Ma. Models of the tectonic setup at chron c4 (~7.5 Ma ago) reproduce the N120° and N150° trends consistent with initial rifting directions. Moreover, the inception of the TR may be explained by failure of the upper plate along a crack that starts at the Gloria fault limit. In the actual tectonic setting the predicted fractures match particularly well the orientation of the LVRs in the second (~N135°–N140°) and third (N150° to N–S) sectors and provide an explanation for the arcuate shape of the TR.

The action of the mantle drag on the base of the brittle plate is a key factor for the development of the more recent LVRs. The timing of predicted fracturing depends on model parameters. For LVR widths of ~10 km the fracture network takes between 1 and 6 Ma to develop, for top mantle viscosities between 5×10^{21} Pa s and 5×10^{22} Pa s respectively. In the best fit model, with a top mantle viscosity of 1×10^{22} Pa s, the fracture network takes ~3 Ma to develop. This is consistent with age determinations in the Azores indicating that LVRs are younger than ~2 Ma. The present tectonic configuration favors the creation of fractures along the Faial Ridge, which according to the results post-date the Terceira Rif. These fractures grow with time but do not reach the MAR. The results are thus in agreement with the present day concentration of tectonic activity in the first LVR sector (comprising Faial, Pico and S. Jorge islands) and with the existing gap at the triple junction region.

Acknowledgments

We thank the comments of an anonymous reviewer that helped to improve the manuscript. This is a contribution from MAREKH, Mid-Atlantic Ridge Evolution in the last 20 Ma between Kurchatov and Hayes, PTDC/MAR/108142/2008.

Appendix A. Modeling formulation

A.1. Numerical method

The solution of any solid mechanics problem needs to satisfy the requirements of the equilibrium, compatibility and constitutive equations, as well as boundary conditions. In the Finite Element Method (FEM) the structure under consideration is discretized into a finite number of elements and nodes. A weak formulation of equilibrium, generally obtained by consideration of the Hamilton's principle or the principle of virtual work, is used to solve the global equilibrium of the structure as a whole, even though this does not necessarily ensure pointwise equilibrium. The general momentum balance equation,

$$-\rho\,\ddot{\mathbf{u}} + \operatorname{div}\sigma = 0 \tag{A.1}$$

where $\ddot{u}$ is the acceleration, ρ the density and σ the stress, can be written in terms of FEM nodal displacements u as (e.g. Bathe, 1996),

$$M\,\ddot{\mathbf{u}} + \mathrm{Ku} = F \tag{A.2}$$

where F is the force vector, K is the stiffness matrix and M is the mass matrix. The weak formulation allows obtaining the equilibrium equations in a fully unified manner, for both quasi-static and dynamic problems. In the absence of inertial forces (quasi-static problems) the momentum equation reduces to the FEM standard equilibrium equation of motion,

$$\mathrm{Ku} = F \tag{A.3}$$

In this work we use the ABAQUS/Explicit dynamic analysis program, which solves Eq. (A.2) using an explicit integration procedure. It can be used to compute quasi-static solutions, provided the loads are applied slowly enough to eliminate inertial effects. At the expense of small time increments, the advantage of the explicit integration scheme is that it overcomes convergence difficulties which arise during strain softening.

A.2. Constitutive equations

The constitutive equation for linear viscoelasticity is that of the standard linear solid (Maxwell viscoelastic rheology). Its representation in the integral form can be derived from an idealized stress relaxation experiment,

$$\sigma^D(t) = 2G(t)\varepsilon_0 \tag{A.4}$$

where at time $t = 0$ the material is subjected to a constant strain ε_0 and the deviatoric stress σ^D is measured as a function of time. $G(t)$ is the shear relaxation modulus function, which can be specified in the form of a two term prony series,

$$G(t) = G_0[1-\exp(-t/\tau)] \tag{A.5}$$

where G_0 is the instantaneous shear modulus and τ is the stress relaxation time. The stress relaxation time is $\tau = \eta/E$ where η is the viscosity and E is the Young's modulus.

Under increasing loads quasi-brittle materials develop a transition from a homogeneous strain field to a heterogeneous strain field with localized regions of intense strain. Continued deformation on the localized regions ultimately lead to rupture of the material and to a decrease in the load carrying capacity widely termed as softening. In this study we follow a general framework for softening prediction and material failure modeling based on damage mechanics (de Borst, 2002; Kachanov, 1993; Lemaitre, 1992). Damage may be described as the progressive physical process by which materials break. It can be studied using a continuum approach that couples damage variables with an elastoplastic model. This coupling is based on the effective stress concept,

$$\tilde{\sigma} = \sigma/(1-D) \tag{A.6}$$

where $\tilde{\sigma}$ is the effective stress and D is a scalar damage variable which represents the degradation of the elastic stiffness. Damage is considered isotropic and bounded by,

$$0 \le D \le 1 \tag{A.7}$$

where $D = 0$ means no damage and $D = 1$ corresponds to a fully broken representative volume element. The constitutive equations for coupled elastoplastic-damage can be derived by application of the strain equivalence principle, which states that "any strain constitutive equation for a damage material may be derived in the same way as for a virgin material except that the usual stress is replaced by the effective stress" (Lemaitre, 1992). The complete set of constitutive equations for coupled elastoplastic damage materials includes the equations for:

a) the undamaged elastoplastic material response
b) the damage initiation criterion and
c) the damage evolution law.

The model response is schematically shown in Fig. A.1. Following the classic elastoplastic behavior, the relation between stress and strain in a damage material is described by,

$$\sigma = (1-D)\mathrm{C} : \varepsilon^e = (1-D)\mathrm{C} : \left(\varepsilon - \varepsilon^{pl}\right) \tag{A.8}$$

where $\mathrm{C} = \mathrm{C}_{ijkl}$ denotes the usual fourth-order isotropic linear-elastic stiffness, ε, ε^e and ε^{pl} denote the strain tensor, its elastic and plastic tensor components respectively. For the prediction of plastic yielding we use the linear associated Drucker–Prager strength criterion. The Drucker–Prager criterion is commonly employed for plastic potential in continuum damage mechanic models (Lee and Fenves, 1998; Lubliner et al., 1989; Wu et al., 2006) and can be written as,

$$\sigma_{\mathrm{eq}} = k - \alpha\sigma_{\mathrm{H}} \tag{A.9}$$

where

$\sigma_{\mathrm{eq}} = \left(\frac{3}{2}\sigma^D_{ij}\sigma^D_{ij}\right)^{1/2}$ is the Von Mises equivalent stress
$\sigma_{\mathrm{H}} = \frac{1}{3}\sigma_{ii}$ is the hydrostatic stress

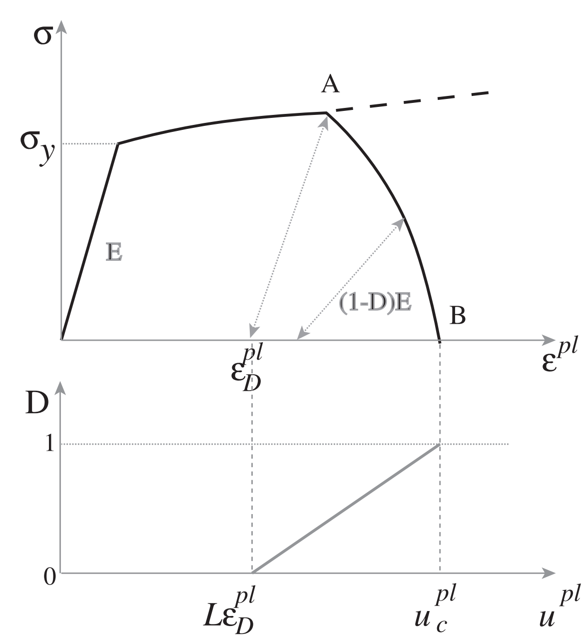

Fig. A.1. Schematic representation of the elastoplastic behavior with progressive damage. The stress–strain curve shows the initial elastic response followed by plastic yielding and damage beyond point A. In point B the material stiffness is fully degraded. E: Young's modulus, σ_y: Plastic yield strength, ε^{pl}_D: plastic strain threshold at the onset of damage. After damage initiation the damage variable D evolves linearly with the effective plastic displacement in the fracture zone. When the effective plastic displacement reaches the value $u^{pl} = u^{pl}_c$ the material is fully degraded (D = 1).

α and k are two material parameters which can be expressed in terms of the Mohr–Coulomb friction angle φ and cohesion stress c_0 (Jiang and Xie, 2011) as,

$$\alpha = 2\sqrt{3}\sin\varphi/(3-\sin\varphi) \text{ and } k = 2\sqrt{3}\cos\varphi\, c_o/(3-\sin\varphi). \tag{A.10}$$

The evolution of the plastic strain is determined by an associated flow rule,

$$\dot{\varepsilon}^{pl} = \dot{\gamma}\partial F/\partial\sigma \tag{A.11}$$

where $\dot{\gamma}\geq 0$ is the plastic multiplier and $F = \sigma_{eq} - k + \alpha\sigma_H$ is the Drucker–Prager yield function. The plastic multiplier is determined using the consistency condition $\dot{F} = 0$.

The damage initiation criterion enforces damage for plastic strains larger than a given threshold ε_D^{pl}. Shear band simulations in 2D usually use a single fixed strain threshold value for the onset of softening which is derived from uniaxial tensile tests (e.g. Buiter et al., 2006; Crook et al., 2006; Ellis et al., 2004). According to Hooputra et al. (2004) the strain threshold under triaxial states of stress is better represented by a function of the stress triaxility (the ratio between the hydrostatic stress and the Von Mises equivalent stress) or by a function of the shear stress ratio θ_s and strain rate $\dot{\varepsilon}$, that is,

$$\varepsilon_D^{pl} = \varepsilon_D^{pl}(\theta_s,\dot{\varepsilon}) \tag{A.12}$$

where

$$\theta_s = \left(\sigma_{eq} - \beta\sigma_H\right)/\tau_{max} \tag{A.13}$$

β is an empirical material parameter and $\tau_{max} = (\sigma_1 - \sigma_3)/2$ is the maximum shear stress. This last criterion derives from a phenomenological fracture model originally intended to predict shear failure in ductile metals, but can be generally applied to fracture due to shear band formation in elastoplastic materials.

The damage evolution law is derived from fracture mechanics concepts and allows modeling the post-localization response. A crack opening law is defined in terms of fracture energy G_f,

$$G_f = \int \sigma du \tag{A.14}$$

where σ and u are the stress and displacement across the fracture process zone, i.e. a small zone in front of the crack tip where the damaging mechanisms take place (de Borst, 2002). A continuum regularization method based on the introduction of a characteristic finite element length (Hillerborg et al., 1976) ensures that the energy dissipation is independent of the mesh size. With the characteristic element length L the evolution of the plastic displacement in the fracture process zone is,

$$\dot{u}^{pl} = L\dot{\varepsilon}^{pl}. \tag{A.15}$$

The evolution of damage can be prescribed by a linear damage evolution law, defined by a straight line lying between two points: $(D = 0, u^{pl} = L\varepsilon_D^{pl})$ at the onset of damage, and $(D = 1, u^{pl} = u_C^{pl})$ at the point of full degradation. It has been shown that a similar continuum regularization method approach can regularize both mode I (tensile crack) and mode II (shear zone) strain localization in quasi-brittle materials (Crook et al., 2006).

A.3. Benchmark problem

To demonstrate the behavior and implementation of the elastoplastic rheology with damage we perform a numerical simulation of shear localization using the model setup of Kaus (2010). The model corresponds to a 2D plane strain section of the elastoplastic crust containing one viscoelastic inclusion of specified length (Fig. A.2). The model is subjected to extension which is implemented via velocity boundary conditions. All the material parameters are listed in Table A.1.

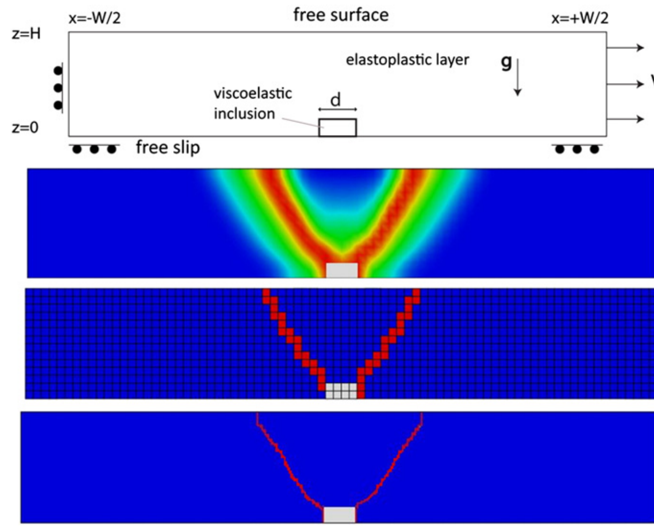

Fig. A.2. Model setup (see Table A.1 for parameters) and results of the numerical benchmark. Shear band formation is depicted as the shear initiation criterion (color banded contour plot where red contours indicate full degradation) or as plots of the damage variable (red elements where D = 1 mark the path of damage propagation). The numerical resolution ((80 × 20) mesh shown and (400 × 100) mesh not shown) does not change the predicted shear band orientation angle of 35°.

The first step in the modeling procedure is to compute the implicit solution of the problem using ABAQUS Standard and the Drucker–Prager rheology without damage. In this way we obtain the static solution prior to strain localization. In problems involving brittle failure there is a sudden drop in the load carrying capacity that generally leads to local instabilities. Convergence difficulties can be avoided by creating a quasi-static analysis using ABAQUS Explicit. In this circumstance loads have to be applied slowly enough to eliminate significant inertia effects. Giving the long time scales of geological processes it is often computationally impractical to explicitly model natural time periods. The way out is to artificially increase the loading rates and check if the inertia forces are still insignificant. Thus, the second step of the modeling procedure is to change the duration of the time step

Table A.1
Parameters used in the benchmark model.

	Parameter	Value
Model setup	Width (W)	20 km
	Height (H)	5 km
	Inclusion size (d)	1 km
	Velocity (Vx)	1 cm yr^{-1}
	Gravity (g)	9.8 m s^{-2}
Viscoelastic layer	Density (ρ)	2700 kg m^{-3}
	Viscosity (η)	1E20 Pa s
	Young's modulus (E)	1E11 Pa
	Poisson's ratio (ν)	0.25
Elastoplastic layer	Density (ρ)	2700 kg m^{-3}
	Young's modulus (E)	1E11 Pa
	Poisson's ratio (ν)	0.25
	Coulomb friction angle (φ)	35°
	Coulomb cohesion (c_0)	50 MPa
	Dilation angle (Ψ)	35°
	Damage initiation criterion $\varepsilon_D^{pl},\theta_s$ (in tabular form)	(0.001,1.8),(0.002,1.9)for$\dot{\varepsilon}\in[0, 1]$, (0.01,2.6)
	Displacement at failure (u_C^{pl})	0.001
Solution control	Loading rate acceleration factor	1.3×10^7 s
	Time of simulation	2500 s (⇔ ~ 1000 yr)
	Explicit time increment (function of resolution)	0.0083 s (80 × 20) 0.0017 s (400 × 100)

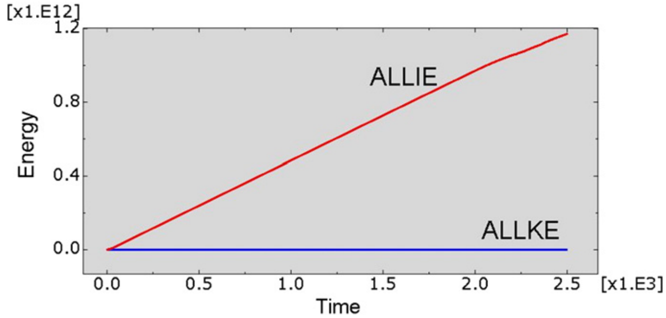

Fig. A.3. Internal (ALLIE) and kinetic (ALLKE) energy from the benchmark calculations of Fig. A.2 using ABAQUS Explicit. The low kinetic energy ensures that dynamical effects are avoided.

and the loading rate and compute the solution in ABAQUS Explicit. After ensuring that the two solutions, the implicit and the explicit, are identical, we proceed with the implementation of the shear fracture damage initiation criterion and the damage evolution law in ABAQUS Explicit.

Given the lack of experimental data on the function $\varepsilon_D^{pl}(\theta_s,\dot{\varepsilon})$ for brittle rocks we perform a first run of the model to assess the set of possible values of θ_s and $\dot{\varepsilon}$. The material parameters in Table 1 are then chosen in such a manner that shear localization occurs starting at the inclusion, as it should. The evolution of damage is prescribed by defining a critical value of the elective plastic displacement u_C^{pl} at which full degradation is reached. The FE models have been made for several numerical resolutions ranging from 80 × 20 to 400 × 100 to and all have the same converging solution (Fig. A.2). However, elements with an aspect ratio close to unity are recommended to avoid mesh alignment effects. The maximum rate of the internal (ALLIE) and kinetic (ALLKE) energy is less than 1E-6, and the maximum ratio of the kinetic and strain energy is less than 0.01, which guarantees that the dynamic effects are negligible (Fig. A.3).

For all the simulated numerical resolutions the predicted shear/damage zones form at an angle of 35° in agreement with the assumed friction angle ($\varphi = 35°$) of the elastoplastic layer. Kaus (2010) points out that at small numerical resolutions (for which the heterogeneity is numerically less well resolved) the orientations of the predicted shear bands are closer to the Arthur angle, $45° \pm (\varphi+/4)$ where Ψ is the dilation angle, whereas at larger resolutions they are closer to the Coulomb angle, $45° \pm (\varphi/2)$. Since we used a well resolved inclusion the numerical benchmark is in agreement with this conclusion.

References

Adam, C., Madureira, P., Miranda, J.M., Lourenço, N., Yoshida, M., Fitzenz, D., 2013. Mantle dynamics and characteristics of the Azores Plateau. Earth Planet. Sci. Lett. http://dx.doi.org/10.1016/j.epsl.2012.11.014.

Bathe, K.J., 1996. Finite Element Procedures. Prentice Hall 1037.

Beier, C., Haase, K., Abouchami, W., Krienitz, M.-S., Hauff, F., 2008. Magma genesis by rifting of oceanic lithosphere above anomalous mantle: Terceira Rift, Azores. Geochem. Geophys. Geosyst. 9, Q12013. http://dx.doi.org/10.1029/2008GC002112.

Bercovici, D., Ricard, Y., Schubert, G., 2001. A two-phase model for compaction and damage: 3. Applications to shear localization and plate boundary formation. J. Geophys. Res. 106, 8925–8940.

Beutel, E., van Wijk, J., Ebinger, C., Keir, D., Agostini, A., 2010. Formation and stability of magmatic segments in the Main Ethiopian and Afar rifts. Earth Planet. Sci. Lett. 293, 225–235.

Buiter, S.J.H., Babeyko, A.Yu., Ellis, S., Gerya, T.V., Kaus, B.J.P., Kellner, A., Schreurs, G., Yamada, Y., 2006. The numerical sandbox: comparison of model results for a shortening and an extension experiment, analogue and numerical modelling of crustal-scale processes. Geol. Soc. Lond. Spec. Publ. 253, 29–64.

Cannat, M., Briais, A., Deplus, C., Escartín, J., Georgen, J., Lin, J., Mercouriev, S., Meyzen, C., Muller, M., Pouliquen, G., Rabain, A., Silva, P., 1999. Mid-Atlantic Ridge–Azores hotspot interactions: along-axis migration of a hotspot-derived event of enhanced magmatism 10 to 40 Ma ago. Earth Planet. Sci. Lett. 173, 257–269.

Crook, A.J.L., Owen, D.R.J., Willson, S.M., Yu, J.G., 2006. Benchmarks for the evolution of shear localisation with large relative sliding in frictional materials. Comput. Methods Appl. Mech. Eng. 195, 991–5010.

de Borst, R., 2002. Fracture in quasi-brittle materials: a review of continuum damage-based approaches. Eng. Fract. Mech. 69 (2), 95–112.

Ellis, S.M., Schreurs, G., Panien, M., 2004. Comparisons between analogue and numerical models of thrust wedge development. J. Struct. Geol. 26 (9), 1659–1675.

Finzi, Y., Muhlhaus, H., Gross, L., Amirbekyan, A., 2012. Shear band formation in numerical simulations applying a continuum damage rheology model. Pure Appl. Geophys. http://dx.doi.org/10.1007/s00024-012-0463-y.

Gente, P., Dyment, J., Maia, M., Goslin, J., 2003. Interaction between the Mid-Atlantic Ridge and the Azores hot spot during the last 85 Ma: emplacement and rifting of the hot spot-derived plateaus. Geochem. Geophys. Geosyst. 4, 8514–8537.

Georgen, J.E., Lin, J., 2002. Three-dimensional passive flow and temperature structure beneath oceanic ridge–ridge–ridge triple junctions. Earth Planet. Sci. Lett. 204, 115–132.

Georgen, J.E., Sankar, R.D., 2010. Effects of ridge geometry on mantle dynamics in an oceanic triple junction region: implications for the Azores Plateau. Earth Planet. Sci. Lett. 298, 23–34.

Goslin, J., Benoit, M., Blanchard, D., Bohn, M., Dosso, L., Dreher, S., Etoubleau, J., Gente, P., Gloaguen, R., Imazu, Y., Luis, J., Maia, M., Merkouriev, S., Oldra, J.-P., Patriat, P., Ravilly, M., Souriot, T., Thirot, J.-L., Yamaashi, T., 1999. Extent of Azores plume influence on the Mid-Atlantic Ridge north of the hotspot. Geology 27, 991–994.

Guest, J.E., Gaspar, J.L., Cole, P.D., Queiroz, G., Duncan, A.M., Wallenstein, N., Ferreira, T., Pacheco, J.-M., 1999. Volcanic geology of Furnas Volcano, São Miguel, Azores. J. Volcanol. Geotherm. Res. 92, 1–29.

Hieronymus, C.F., 2004. Control on seafloor spreading geometries by stress- and strain-induced lithospheric weakening. Earth Planet. Sci. Lett. 222, 177–189.

Hildenbrand, A., Marques, F.O., Costa, A.C.G., Sibrant, A.L.R., Silva, P.F., Henry, B., Miranda, J.M., Madureira, P., 2012. Reconstructing the architectural evolution of volcanic islands from combined K/Ar, morphologic, tectonic, and magnetic data: the Faial Island example (Azores). J. Volcanol. Geotherm. Res. 241, 39–48.

Hillerborg, A., Modéer, M., Petersson, P.E., 1976. Analysis of crack formation and crack growth in concrete by means of fracture mechanics and finite elements. Cem. Concr. Res. 6, 773–782.

Hooputra, H., Gese, H., Del, H., Werner, H., 2004. A comprehensive failure model for crashworthiness simulation of aluminium extrusions. Int. J. Crashworthiness 9 (5), 449–463.

Jiang, H., Xie, Y., 2011. A note on the Mohr–Coulomb and Drucker–Prager strength criteria. Mech. Res. Commun. 38 (4), 309–314.

Johnson, C.L., Wijbrans, J.R., Constable, C.G., Gee, J., Staudigel, H., Tauxe, L., Forjaz, V.H., Salgueiro, M., 1998. $^{40}Ar/^{39}Ar$ ages and paleomagnetism of São Miguel lavas, Azores. Earth Planet. Sci. Lett. 160, 637–649.

Kachanov, M., 1993. Elastic solids with many cracks and related problems. In: Hutchinson, J., Wu, T. (Eds.), Advances in Applied Mechanics, 30, pp. 259–445.

Kaus, B.J.P., 2010. Factors that control the angle of shear bands in geodynamic numerical models of brittle deformation. Tectonophysics 484 (1–4), 36–47.

Keir, D., Ebinger, C.J., Stuart, G.W., Daly, E., Ayele, A., 2006. Strain accommodation by magmatism and faulting as rifting proceeds to breakup: seismicity of the northern Ethiopian rift. J. Geophys. Res. 111, B05314. http://dx.doi.org/10.1029/2005JB003748.

Lachenbruch, A.H., 1973. A simple mechanical model for oceanic spreading centers. J. Geophys. Res. 78, 3395–3417.

Lee, J., Fenves, G.L., 1998. Plastic-damage model for cyclic loading of concrete structures. J. Eng. Mech. Div. ASCE 124, 892–900.

Lemaitre, J., 1992. A Course on Damage Mechanics, 2nd ed. Springer Verlag, New York (262 pp.).

Lin, J., Parmentier, E.M., 1990. A finite amplitude necking model of rifting in brittle lithosphere. J. Geophys. Res. 95, 4909–4923.

Lourenço, N., 2007. Tectono-magmatic Processes at the Azores Triple Junction. Ph.D. Dissertation Universidade do Algarve (239 pp.).

Lourenço, N., Miranda, J.M., Luis, J.F., Ribeiro, A., Mendes-Victor, L.A., Madeira, J., Needham, H.D., 1998. Morpho-tectonic analysis of the Azores Volcanic Plateau from a new bathymetric compilation of the area. Mar. Geophys. Res. 20, 141–156.

Lubliner, J., Oliver, S., Oñate, E., 1989. A plastic-damage model for concrete. Int. J. Solids Struct. 25 (2), 299–326.

Luis, J.F., Miranda, J.M., 2008. Re-evaluation of magnetic chrons in the North-Atlantic between 35 N and 47 N: implications for the formation of the Azores triple junction and associated plateau. J. Geophys. Res. 113, B10105.

Luis, J.F., Neves, M.C., 2006. The isostatic compensation of the Azores Plateau: a 3D admittance and coherence analysis. J. Volcanol. Geotherm. Res. 156, 10–22.

Luis, J.F., Miranda, J.M., Patriat, P., Galdeano, A., Rossignol, J.C., Mendes-Victor, L., 1994. Açores Triple Junction evolution in the last 10 Ma from a new aeromagnetic survey. Earth Planet. Sci. Lett. 125, 439–459.

Lyakhovsky, V., Ben-Zion, Y., Agnon, A., 1997. Distributed damage, faulting, and friction. J. Geophys. Res. 102, 27635–27649.

Miranda, J.M., Luis, J.F., Lourenço, N., Fernandes, R., Neves, C., 2011. Evolution of the segmentation pattern of the Mid-Atlantic Ridge between 20 N and 41 N, in the last 25 Ma. Geophys. Res. Abstr. 13 (EGU2011-12181).

Miranda, J.M., Luis, J.F., Lourenço, N., Fernandes, R.M.S., 2013. The structure and evolution of the Azores triple junction based on bathymetric, magnetic and geodetic data: implications for S. Miguel Island. J. Geol. Soc. (in press).

Navarro, A., Lourenço, N., Chorowicz, J., Miranda, J.M., Catalão, J., 2009. Analysis of geometry of volcanoes and faults in Terceira Island (Azores): evidence for reactivation tectonics at the EUR/AFR plate boundary in the Azores triple junction. Tectonophysics 465, 98–113.

Neves, M.C., Bott, M.H.P., Searle, R.C., 2004. The effect of seafloor subsidence on the stress field at mid-ocean ridge offsets. Tectonophysics 386, 223–242.

Parsons, B.E., Sclater, J.G., 1977. An analysis of the variation of ocean floor bathymetry and heat flow with age. J. Geophys. Res. 82, 803–827.

Rudnicki, J.W., Rice, J.R., 1975. Conditions for the localization of deformation in pressure-sensitive dilatant materials. J. Mech. Phys. Solids 23, 371–394.

Saemundsson, K., 1986. Subaerial volcanism in the western Atlantic. In: Vogt, P.R., Tucholke, B.E. (Eds.), The Western North Atlantic Region, vol. M. The Geology of North America, The Geological Society of America, Boulder, CO, pp. 69–86.
Schilling, J.-G., 1975. Azores mantle blob: rare-earth evidence. Earth Planet. Sci. Lett. 25, 103–115.
Silva, P.F., Henry, B., Marques, F.O., Hildenbrand, A., Madureira, P., Mériaux, C., Kratinová, Z., 2012. Palaeomagnetic study of a sub-aerial volcanic ridge (São Jorge Island, Azores) for the past 1.3 Myr: evidence for the Cobb Mountain Subchron, volcano flank instability and tectono-magmatic implications. Geophys. J. Int. 188, 959–978.
Silveira, G., Vinnik, L., Stutzmann, E., Farra, V., Kiselev, S., Morais, I., 2010. Stratification of the Earth beneath the Azores from P and S receiver function. Earth Planet. Sci. Lett. 299, 91–103.
Stretch, R.C., Mitchell, N.C., Portaro, R.A., 2006. A morphometric analysis of the submarine volcanic ridge south-east of Pico Island, Azores. J. Volcanol. Geotherm. Res. 156, 35–54.
Ten Brink, U., 1991. Volcano spacing and plate rigidity. Geology 19, 397–400.
Vogt, P.R., Jung, W.Y., 2004. The Terceira Rift as hyper-slow, hotspot-dominated oblique spreading axis: a comparison with other slow-spreading plate boundaries. Earth Planet. Sci. Lett. 218, 77–90.
Wu, J.Y., Li, J., Faria, R., 2006. An energy release rate-based plastic-damage model for concrete. Int. J. Solids Struct. 43, 583–612.
Yang, T., Shen, Y., van der Lee, S., Solomon, S.C., Hung, S., 2006. Upper mantle structure beneath the Azores hotspot from finite-frequency seismic tomography. Earth Planet. Sci. Lett. 250, 11–26.